


Investigation of the structure and magnetism in lanthanide β -triketonate tetranuclear assemblies

Brodie L. Reid, Robert C. Woodward, Rebecca O. Fuller, Alexandre N. Sobolev, Brian W. Skelton, Mark I. Ogden & Massimiliano Massi

To cite this article: Brodie L. Reid, Robert C. Woodward, Rebecca O. Fuller, Alexandre N. Sobolev, Brian W. Skelton, Mark I. Ogden & Massimiliano Massi (2016): Investigation of the structure and magnetism in lanthanide β -triketonate tetranuclear assemblies, Journal of Coordination Chemistry, DOI: [10.1080/00958972.2016.1180375](https://doi.org/10.1080/00958972.2016.1180375)

To link to this article: <http://dx.doi.org/10.1080/00958972.2016.1180375>

 View supplementary material 

 Accepted author version posted online: 21 Apr 2016.
Published online: 05 May 2016.

 Submit your article to this journal 

 Article views: 23

 View related articles 

 View Crossmark data 

Investigation of the structure and magnetism in lanthanide β -triketonate tetranuclear assemblies

Brodie L. Reid^a, Robert C. Woodward^b, Rebecca O. Fuller^c, Alexandre N. Sobolev^d, Brian W. Skelton^d, Mark I. Ogden^a and Massimiliano Massi^a

^aDepartment of Chemistry and Nanochemistry Research Institute, Curtin University, Bentley, Australia; ^bSchool of Physics, The University of Western Australia, Crawley, Australia; ^cChemistry M310, School of Chemistry and Biochemistry, University of Western Australia, Crawley, Australia; ^dCentre for Microscopy, Characterisation and Analysis, University of Western Australia, Crawley, Australia

ABSTRACT

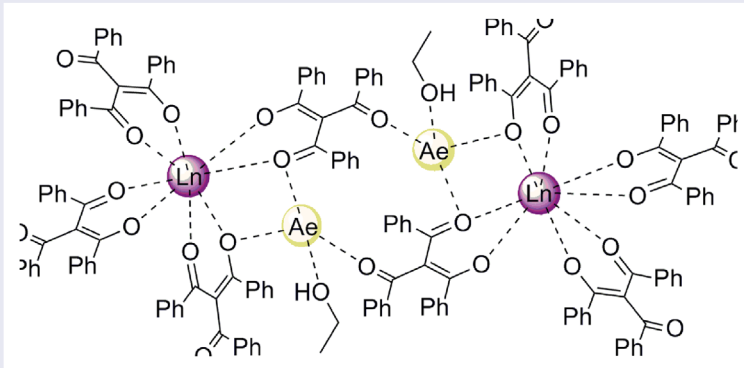
The preparation of discrete tetranuclear lanthanide/alkali metal (Ae) assemblies bearing a tribenzoylmethane ligand (LH) is discussed. These assemblies have the general formula $[\text{Ln}(\text{Ae-HOEt})(\text{LH})_4]_2$, where $\text{Ln}^{3+} = \text{Gd}^{3+}$, Tb^{3+} , Dy^{3+} , Ho^{3+} and $\text{Ae}^+ = \text{Na}^+$, K^+ , Rb^+ . The coordination geometries of the lanthanide species were analyzed and compared, revealing a trend between an eight-coordinate square antiprism and triangular dodecahedron dependent on the nature of lanthanide, alkali metal, and lattice solvent. The potassium-containing analogs were also analyzed for their magnetic susceptibility.

ARTICLE HISTORY

Received 6 January 2016
Accepted 23 March 2016


KEYWORDS


Lanthanides; magnetism; triketonates; diketonates; assemblies



1. Introduction

Coordination complexes of the trivalent lanthanide ions have been extensively investigated due to the intrinsic magnetic and optical properties arising from the 4f-electrons. The interest is well justified by the many technological applications found by lanthanide-containing compounds, spanning optical displays [1–3], telecommunication devices [4, 5], magnets [6] as well as diagnostic and therapeutic medicinal agents [7, 8]. In this field, the β -diketonate class of ligands is certainly ubiquitous, due to

CONTACT Mark I. Massimiliano Ogden Massi  m.ogden@curtin.edu.au

 Supplemental data for this article can be accessed <http://dx.doi.org/10.1080/00958972.2016.1180375>.

© 2016 Informa UK Limited, trading as Taylor & Francis Group

their ability to efficiently bind oxophilic trivalent lanthanide ions forming relatively stable complexes. β -Diketonate ligands are also known to stabilize various structural motifs when binding to lanthanide cations, ranging from mononuclear complexes to extended oxo/hydroxo clusters obtained via the established "controlled hydrolysis" synthesis [9–12].

Given the enormous research effort on lanthanide β -diketonate complexes, it is rather surprising that the analogous β -triketonate complexes have received scarce attention [13–15]. This is even more remarkable considering that β -triketonate ligands are synthetically accessible via facile Claisen-type condensations from β -diketonate ligands.

We recently initiated an investigation focused on evaluating the coordination chemistry and optical properties of lanthanide β -triketonate complexes using the tribenzoylmethane ligand. Our studies revealed the formation of discrete $\text{Ln}^{3+}/\text{Ae}^+$ tetranuclear assemblies of the general formula $[\text{Ln}(\text{Ae-HOEt})(\text{L})_4]_2$, where $\text{Ln}^{3+} = \text{Eu}^{3+}, \text{Er}^{3+}, \text{ and } \text{Yb}^{3+}$; $\text{Ae}^+ = \text{Na}^+, \text{K}^+, \text{ and } \text{Rb}^+$ [16, 17]. This family of compounds proved to be remarkably robust to variations of the identity of the lanthanide as well as the alkali metal cations. Our work was initially focused on investigation of the photophysical properties of these assemblies, thus using red emitting Eu^{3+} cations and near-infrared emitting Er^{3+} and Yb^{3+} cations. We have now continued our research effort to extend the family of these assemblies including the lanthanide ions $\text{Gd}^{3+}, \text{Tb}^{3+}, \text{Dy}^{3+}, \text{ and } \text{Ho}^{3+}$. Furthermore, we have started a preliminary investigation of their magnetic properties. Molecular magnets being developed around single lanthanide nuclei with large ground spin states use the inherent magnetic anisotropy and ligand field symmetry to produce the desired slow magnetic relaxation. More recently, dinuclear lanthanide complexes have also been shown to exhibit desirable properties. However, unlike their mononuclear counterparts, these complexes tend to have strong magnetic-exchange interactions through a radical bridging atom [18, 19].

2. Results and discussion

2.1. Synthesis

Tribenzoylmethane **LH** was synthesized according to our previously reported procedure [16], in which dibenzoylmethane was reacted with benzoyl chloride and NaH in diethyl ether. The preparation of the $\text{Ln}^{3+}/\text{Ae}^+$ tetranuclear assemblies, $[\text{Ln}(\text{Ae-HOEt})(\text{L})_4]_2$ (in this case $\text{Ln}^{3+} = \text{Gd}^{3+}, \text{Tb}^{3+}, \text{Dy}^{3+}, \text{Ho}^{3+}$; $\text{Ae}^+ = \text{K}^+, \text{Rb}^+$), was analogous to our previously reported procedure [16, 17], whereby four equivalents of **LH** and AeOH were reacted with one equivalent of hydrated LnCl_3 in ethanol (figure 1). The synthesis of the $[\text{Tb}(\text{Na-HOEt})(\text{L})_4]_2$ tetranuclear assembly is also reported herein, using NaOH. The targeted assemblies were in general characterized by IR spectroscopy and elemental analysis. In particular, the latter proved in some cases difficult to obtain, as the assemblies have the tendency to co-crystallize as solvates containing various degrees of lattice solvent molecules. This characteristic is analogous to the previously reported assemblies of $\text{Eu}^{3+}, \text{Er}^{3+}$ and Yb^{3+} . While the preparation of these assemblies was

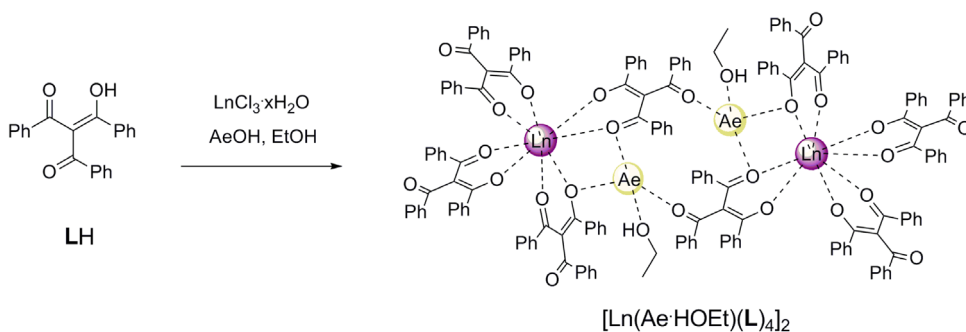


Figure 1. Synthetic pathway to lanthanide assemblies bearing β -triketonate ligands. $\text{Ln}^{3+} = \text{Gd}^{3+}, \text{Tb}^{3+}, \text{Dy}^{3+}, \text{Ho}^{3+}$; $\text{Ae}^+ = \text{K}^+, \text{Rb}^+$.

attempted with all the lanthanide ions, their isolation with elements lighter than Eu^{3+} has proven to be unsuccessful to date.

2.2. X-ray diffraction

As found previously [16, 17], the tetranuclear $[\text{Ln}(\text{Ae-HOEt})(\text{L})_4]_2$ assemblies are neutral discrete species whereby both Ln^{3+} cations are eight-coordinate by four bis-chelating β -triketonate ligands. A dimer is formed through coordination of an alkali metal through the third keto arm of one β -triketonate molecule (see figure 2 for $[\text{Tb}(\text{K-HOEt})(\text{L})_4]_2$ structure; see Supporting Information for all other structures).

Although each of the isolated $[\text{Ln}(\text{Ae-HOEt})(\text{L})_4]_2$ assemblies are analogous in structure, it was determined that, in addition to unsolvated structures, the assemblies can also crystallize as a different solvate, $[\text{Ln}(\text{Ae-HOEt})(\text{L})_4]_2 \cdot 2(\text{EtOH})$. In fact, for the $[\text{Dy}(\text{K-HOEt})(\text{L})_4]_2$ assembly, both unsolvated and solvated structures were identified by single crystal X-ray diffraction from the same crystallization vial. This behavior was also previously observed for the $\text{Yb}^{3+}/\text{K}^+$ assembly [16, 17]. Table 1 describes each of the assemblies presented as their crystallized species, as well as an abbreviation to describe each assembly, $\{\text{Ln}_2\text{Ae}_2\}$, which will be used to denote the assemblies throughout the manuscript. The assemblies are essentially isomorphous when their structures possess the same degree of solvation, irrespective of the identity of the lanthanide and/or alkali metal cations.

Selected distances are given in table 2 for each assembly, including average Ln-O distances and $\text{Ln} \cdots \text{Ln}$ distances. The average Ln-O distance for all assemblies decreases from Tb^{3+} ($\sim 2.36 \text{ \AA}$) to Ho^{3+} ($\sim 2.33 \text{ \AA}$), consistent with considerations based on the lanthanide contraction. The $\text{Ln} \cdots \text{Ln}$ distance in each of the assemblies were affected by the lanthanide contraction, but also the presence (or absence) of solvent molecules and the identity of the alkali metal. The lanthanide contraction gives a general decrease in the intramolecular $\text{Ln} \cdots \text{Ln}$ distance.

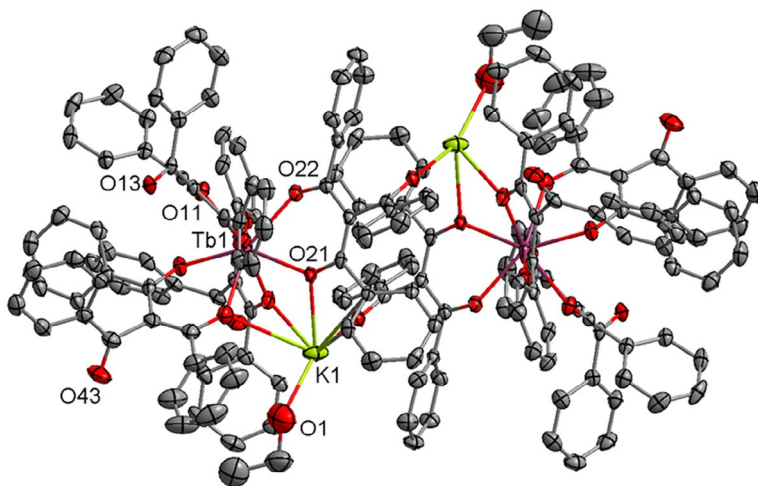


Figure 2. Molecular plot of the $[\text{Tb}(\text{K-HOEt})(\text{L})_4]_2$ assembly with displacement ellipsoids at the 50% probability level.

Table 1. Tetranuclear assemblies sorted by their isomorphous crystallized structures.

Formulation	$\{\text{Ln}_2\text{Ae}_2\}$ assemblies
$[\text{Ln}(\text{Na-HOEt})(\text{L})_4]_2$	$\{\text{Tb}_2\text{Na}_2\}$
$[\text{Ln}(\text{K/Rb-HOEt})(\text{L})_4]_2$	$\{\text{Tb}_2\text{K}_2\}, \{\text{Dy}_2\text{K}_2\}, \{\text{Ho}_2\text{K}_2\}$
$[\text{Ln}(\text{Ae-HOEt})(\text{L})_4]_2 \cdot 2\text{EtOH}$	$\{\text{Tb}_2\text{Rb}_2\}, \{\text{Gd}_2\text{K}_2\}, \{\text{Gd}_2\text{Rb}_2\}, \{\text{Dy}_2\text{K}_2\}, \{\text{Dy}_2\text{Rb}_2\}, \{\text{Ho}_2\text{Rb}_2\}$

Table 2. Selected distances (Å) between the two lanthanide cations (Ln···Ln) within the tetranuclear assemblies, and average Ln–O bond distances within the first coordination sphere. Structures are grouped by their formulation.

Formulation	Assembly	Ln···Ln	Ave. Ln–O
[Ln(Na·HOEt)(L) ₄] ₂	{Tb ₂ Na ₂ }	8.9547(4)	2.354
[Ln(K/Rb·HOEt)(L) ₄] ₂	{Tb ₂ K ₂ }	8.8380(5)	2.358
	{Dy ₂ K ₂ }	8.8207(4)	2.344
	{Ho ₂ K ₂ }	8.8033(2)	2.332
	{Tb ₂ Rb ₂ }	8.9374(1)	2.357
[Ln(Ae·HOEt)(L) ₄] ₂ ·2EtOH	{Gd ₂ K ₂ }	8.9664(5)	2.369
	{Gd ₂ Rb ₂ }	8.9514(5)	2.372
	{Dy ₂ K ₂ }	8.9461(4)	2.344
	{Dy ₂ Rb ₂ }	8.9214(2)	2.343
	{Ho ₂ Rb ₂ }	8.9076(4)	2.330

This trend is only comparable within each formulation, and thus the position of the alkali metal-bound ethanol has a profound effect on the packing of the tetranuclear assemblies and the Ln···Ln distance. Furthermore, the presence of the K⁺ or Rb⁺ presents some anomalies in the lanthanide contraction trend, which is not unexpected due to the larger size of Rb⁺ compared to K⁺.

The coordination geometries of all species were assessed using Shape Version 2.1 software [20, 21] and have continuous shape measures (CShM) best describing a square antiprism or a triangular dodecahedron polyhedron (see Supporting Information for CShM values).

These CShM values were plotted on a shape map together with the CShM values of our previously reported assemblies [17] (figure 3, for CShM values of our previously reported assemblies – see the literature [17]). The shape map illustrates clearly that a variety of CShM clusters emerges. The presence (or absence) of the lattice solvent molecules and the identity of the Ae⁺ cation have an influence on the specific geometry of the coordination environment around the lanthanide center. These clusters correspond to the assemblies within the different crystallized formulations such as those described previously.

The major factor contributing to the coordination geometry seems to be the degree of solvation and nature of the lattice solvent molecules. The [Ln(Na·HOEt)(L)₄]₂ (**I**) species have a coordination geometry that is closest to a square antiprism, irrespective of the lanthanide cation. The deviation from the lowest energy interconversion pathway (LEIP, black line in figure 4) increases from the smaller Yb³⁺ to the larger Eu³⁺, indicating a distortion away from the regular polyhedra with increasing lanthanide size.

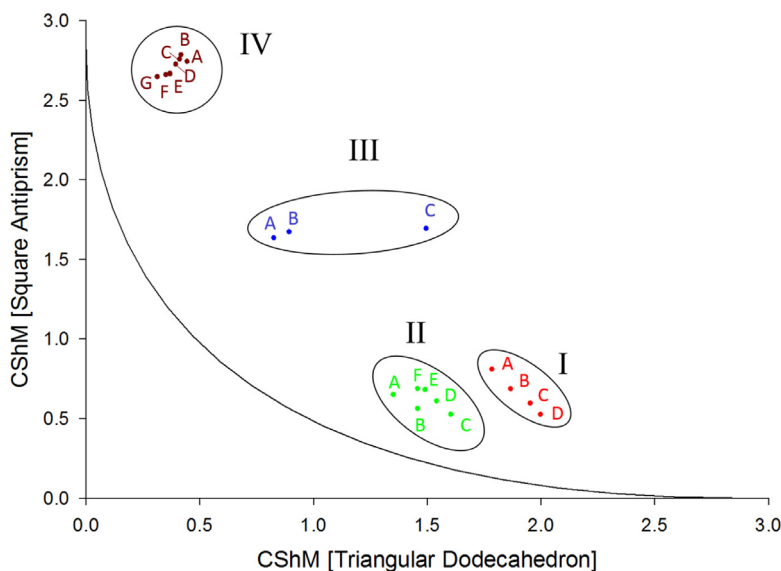
From this arrangement, a slight distortion is observed for [Ln(K/Rb·HOEt)(L)₄]₂ (**II**) structures; however, the coordination sphere is again best described by a square antiprism geometry. The deviation from the LEIP follows the same trend as the [Ln(Na·HOEt)(L)₄]₂ structures which increases with increasing lanthanide size from {Yb₂K₂} to {Tb₂K₂}.

Further distortion is evident for the previously reported [Ln(Ae·HOEt)(L)₄]₂·2(H₂O)(EtOH) (**III**) structures [17]. The deviation trend is again consistent from {Yb₂K₂} to {Er₂K₂}.

Better described as a triangular dodecahedron, the [Ln(Ae·HOEt)(L)₄]₂·2(EtOH) (**IV**) assemblies are with two lattice ethanol molecules. Again, the deviation from the LEIP increases with increasing lanthanide size, from {Ho₂Rb₂} to {Eu₂K₂}. In the solvated (**IV**) series, the presence of K⁺ or Rb⁺ appears to affect the deviation from regular polyhedra to a lesser extent. This observation is most likely due to the fact that the investigated structures now include larger lanthanides, whose coordination geometry is less affected by the size of the alkali metal.

2.3. Static magnetic properties

Static magnetic properties for the K⁺ containing assemblies were investigated (figure 4). The $\chi_{\text{M}}T$ product for {Gd₂K₂} assembly decreases slightly from the room temperature value of 14.1–11.9 cm³ K mol⁻¹ at 20 K. This value is slightly lower than the expected 15.7 cm³ K mol⁻¹ spin only value for two uncoupled Gd ions ($S = 7/2$, $^8S_{7/2}$, $g = 2$). The susceptibility product then remains relatively constant below 20 K.



[Ln(Na·HOEt)(L) ₄] ₂ (I)	[Ln(K/Rb·HOEt)(L) ₄] ₂ (II)	[Ln(Ac·HOEt)(L) ₄] ₂ ·2(H ₂ O) (EtOH) (III)	[Ln(Ac·HOEt)(L) ₄] ₂ ·2(EtOH) (IV)
A: {Eu ₂ Na ₂ }	A: {Er ₂ Rb ₂ }	A: {Yb ₂ K ₂ }	A: {Eu ₂ K ₂ }
B: {Tb ₂ Na ₂ }	B: {Yb ₂ Rb ₂ }	B: {Er ₂ K ₂ }	B: {Eu ₂ Rb ₂ }, {Gd ₂ K ₂ }
C: {Er ₂ Na ₂ }	C: {Yb ₂ K ₂ }	C: {EuK·BuOH}	C: {Gd ₂ Rb ₂ }
D: {Yb ₂ Na ₂ }	D: {Ho ₂ K ₂ }		D: {Dy ₂ K ₂ }
	E: {Tb ₂ K ₂ }		E: {Tb ₂ Rb ₂ }
	F: {Dy ₂ K ₂ }		F: {Dy ₂ Rb ₂ }
			G: {Ho ₂ Rb ₂ }

Figure 3. Top: Shape map presenting the CShM of the 21 lanthanide/alkali metal assemblies presented previously and herein, against the reference square antiprism and triangular dodecahedron polyhedra. The black trace represents the lowest energy interconversion pathway (LEIP) between the two reference polyhedra. Classes of assemblies are circled and the class number printed alongside. Bottom: the legend is shown in the table. Bolded formulations are reported in this manuscript, whereas italicized formulations have been reported elsewhere [16, 17].

The room temperature value of $\chi_M T$ 28.3 cm³ K mol⁻¹ for the {Dy₂K₂} is within experimental error of the expected values of 28.2 cm³ K mol⁻¹ for two uncoupled Dy³⁺ ions ($S = 5/2$, $L = 5$, $^6H_{15/2}$). However $\chi_M T$ for the {Tb₂K₂} (20.1 cm³ K mol⁻¹) and {Ho₂K₂} (21.1 cm³ K mol⁻¹) are lower than the expected values for two uncoupled Tb³⁺ ($S = 3$, $L = 3$, 7F_6 23.6 cm³ K mol⁻¹) or Ho³⁺ ($S = 2$, $L = 4$, $^5I_{15/2}$ 28 cm³ K mol⁻¹) ions. As temperature is lowered, $\chi_M T$ decreases gradually. This decrease is likely the result of depopulation of the excited Stark levels and the exchange interaction between atoms [22]. At lower temperatures this decrease is more rapid, likely the result of the crystal field effect [23] or the presence of weak antiferromagnetic interactions between the atoms.

The field dependence of the magnetization (figure 5) exhibits a fast increase in weak fields. When larger fields are applied the magnetization only increases slowly for {Gd₂K₂}, {Dy₂K₂} and {Ho₂K₂}. For {Dy₂K₂} and {Ho₂K₂} the slow rise is likely due to the magnetic anisotropy associated with the Dy and Ho ions. Further increasing the field results in saturation of the magnetization for both the {Gd₂K₂} and {Dy₂K₂}. For {Dy₂K₂} the value deviates significantly from the theoretical saturation. The magnetization

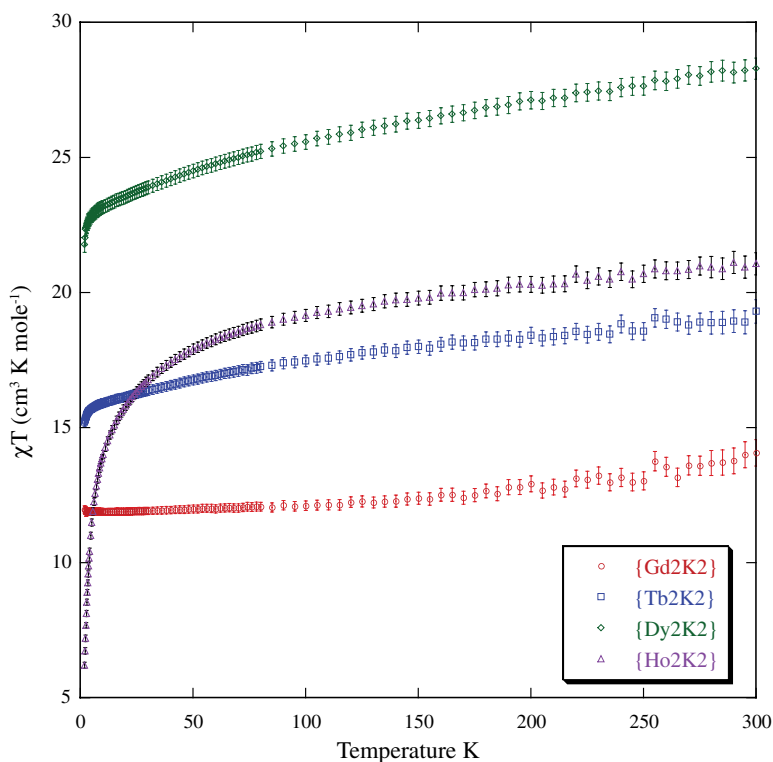


Figure 4. The temperature-dependent $\chi_M T$ profiles in a 100 Oe field for the $\{Gd_2K_2\}$ (red), $\{Dy_2K_2\}$ (green), $\{Tb_2K_2\}$ (blue) and $\{Ho_2K_2\}$ (pink) assemblies (see <http://dx.doi.org/10.1080/00958972.2016.1180375> for color version).

continues to increase for $\{Tb_2K_2\}$ and $\{Ho_2K_2\}$ complexes at 7 T. The smaller than expected values measured at 7 T supports the occurrence of both magnetic anisotropy and ligand field induced splitting of the Stark Levels [22].

3. Conclusion

The sequence of tetranuclear Ln^{3+}/Ae^+ assemblies reported here confirms that the tribenzoylmethane ligand can support the formation of these species for the lanthanide cations ranging from Eu^{3+} to Yb^{3+} , with efforts to obtain crystalline products for the lighter lanthanides being unsuccessful. The different solvates obtained have a significant influence on the coordination sphere geometry of the lanthanide centers, but the specific solvate obtained is not strongly influenced by the nature and size of the lanthanide cations, as illustrated by the isolation of two different Dy^{3+}/K^+ solvates. The magnetic properties of the complexes reported here are not entirely as expected, especially in considering the values of $\chi_M T$ for some of the isolated assemblies. Deviations observed are tentatively ascribed to the presence of various solvates, and crystal field effects, in the bulk samples.

4. Experimental

4.1. General procedures

All reagents and solvents were purchased from chemical suppliers and used as received. The ligand, 2-benzoyl-1,3-diphenyl-1,3-propanone (LH), was prepared as we previously reported [16]. Hydrated $LnCl_3$ was prepared by reaction of Ln_2O_3 with hydrochloric acid (5 M) [24], followed by evaporation of

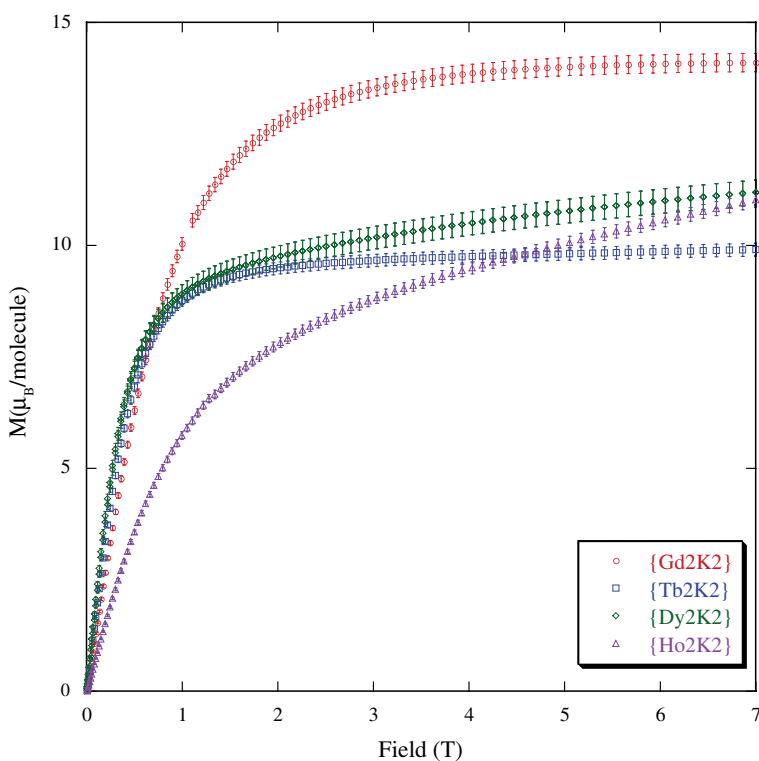


Figure 5. Field-dependent M vs. H/T plots at 2 K for the $\{\text{Gd}_2\text{K}_2\}$ (red), $\{\text{Dy}_2\text{K}_2\}$ (green), $\{\text{Tb}_2\text{K}_2\}$ (blue) and $\{\text{Ho}_2\text{K}_2\}$ (pink) assemblies (see <http://dx.doi.org/10.1080/00958972.2016.1180375> for color version).

the solvent under reduced pressure. Infrared spectra (IR) were recorded on solid-state samples using an attenuated total reflectance Perkin Elmer Spectrum 100 FT-IR from 4000 to 650 cm^{-1} . Melting points were determined using a BI Barnsted Electrothermal 9100 apparatus. Elemental analyses were obtained at either Curtin University or the University of Tasmania.

4.2. Magnetic measurements

Magnetization measurements were performed using a Quantum Design MPMS3 SQUID magnetometer. Temperature-dependent magnetic susceptibility measurements were made on powdered polycrystalline samples suspended in eicosane for the $\{\text{Tb}_2\text{K}_2\}$, $\{\text{Dy}_2\text{K}_2\}$, $\{\text{Ho}_2\text{K}_2\}$ and $\{\text{Gd}_2\text{K}_2\}$ assemblies in an applied field of 100 Oe from 2 to 300 K. In addition, magnetization curves in fields up to 7 T were measured at 2 K. Results have been corrected for the diamagnetism of the sample holder, eicosane and ligand.

4.3. General synthesis of $[\text{Ln}(\text{Ae}\cdot\text{HOR})(\text{L})_4]_2$

To a mixture of LH (68–72 mg, 0.21 mmol) and hydrated LnCl_3 (20 mg), an aqueous AeOH solution ($\text{Ae}^+ = \text{Na}^+, \text{K}^+, \text{Rb}^+$; 1 M, 206–218 μL , 0.21 mmol) was added. Ethanol (10 mL) was added and the mixture heated at reflux for 30 min. The resulting mixture was hot filtered and the filtrate left to stand at RT. Slow evaporation of the solvent over several days afforded yellow crystals (10–40 mg).

4.3.1. $[\text{Gd}(\text{K}\cdot\text{HOEt})(\text{L})_4]_2$

M.p. 269–270 $^\circ\text{C}$; elemental Anal. Calcd (%) for $\text{C}_{180}\text{H}_{132}\text{Gd}_2\text{K}_2\text{O}_{26}\cdot 0.5(\text{H}_2\text{O})$: C, 69.46; H, 4.31; found: C, 69.05; H, 4.05; ATR-IR: $\nu = 3642 \text{ w}, 3567 \text{ w}, 3057 \text{ w}, 3027 \text{ w}, 1645 \text{ m}, 1609 \text{ w}, 1583 \text{ s}, 1543 \text{ s}, 1491 \text{ m}, 1447$

m, 1368 s, 1311 m, 1277 m, 1178 w, 1150 m, 1073 w, 1027 w, 1013 w, 999 w, 928 w, 897 m, 823 w, 780 w, 745 m, 694 m, 668 cm⁻¹ w.

4.3.2. [Gd(Rb-HOEt)(L)₄]₂

M.p. 263–264 °C; elemental Anal. Calcd (%) for C₁₈₀H₁₃₂Gd₂Rb₂O₂₆: C, 67.64; H, 4.16; found: C, 67.65; H, 3.51; the elemental analysis deviates somewhat from the theoretical values, possibly due to the presence of multiple solvates; ATR-IR: $\nu = 3650$ w, 3571 w, 3057 w, 3021 w, 1645 m, 1610 w, 1584 s, 1543 s, 1491 m, 1448 m, 1369 s, 1311 m, 1278 m, 1179 w, 1151 m, 1074 w, 1027 w, 1013 w, 999 w, 925 w, 898 m, 823 w, 812 w, 780 w, 747 m, 694 m, 669 cm⁻¹ w.

4.3.3. [Tb(Na-HOEt)(L)₄]₂

M.p. 262–263 °C; elemental Anal. Calcd (%) for C₁₈₀H₁₃₂Tb₂Na₂O₂₆: C, 70.31; H, 4.33; found: C, 69.74; H, 4.33; elemental analysis deviates somewhat from the theoretical values, possibly due to the presence of multiple solvates; ATR-IR: $\nu = 3644$ w, 3557 w, 3058 w, 3032 w, 1645 m, 1584 s, 1543 s, 1491 m, 1448 m, 1369 s, 1311 m, 1278 m, 1179 w, 1150 m, 1073 w, 1027 w, 1013 w, 999 w, 974 w, 923 w, 898 m, 823 w, 780 w, 746 m, 694 m, 669 cm⁻¹ w.

4.3.4. [Tb(K-HOEt)(L)₄]₂

M.p. 239–241 °C; elemental Anal. Calcd (%) for C₁₈₀H₁₃₂Tb₂K₂O₂₆·1.5(H₂O): C, 68.98; H, 4.34; found: C, 68.50; H, 3.83; elemental analysis deviates somewhat from the theoretical values, possibly due to the presence of multiple solvates; ATR-IR: $\nu = 3648$ w, 3567 w, 3057 w, 3024 w, 1645 m, 1609 w, 1584 s, 1542 s, 1491 m, 1448 m, 1368 s, 1311 m, 1277 m, 1179 w, 1151 m, 1073 w, 1027 w, 1013 w, 999 w, 975 w, 929 w, 897 m, 823 w, 780 w, 747 m, 694 m, 669 cm⁻¹ w.

4.3.5. [Tb(Rb-HOEt)(L)₄]₂

M.p. 263–264 °C; elemental Anal. Calcd (%) for C₁₈₀H₁₃₂Tb₂Rb₂O₂₆·3(H₂O): C, 66.44; H, 4.27; found: C, 66.13; H, 3.35; the elemental analysis deviates somewhat from the theoretical values, possibly due to the presence of multiple solvates; ATR-IR: $\nu = 3650$ w, 3575 w, 3056 w, 3024 w, 1644 m, 1609 w, 1584 s, 1544 s, 1491 m, 1447 m, 1369 s, 1311 m, 1276 m, 1179 w, 1153 m, 1073 w, 1027 w, 1013 w, 999 w, 925 w, 897 m, 824 w, 780 w, 748 m, 694 m, 669 cm⁻¹ w.

4.3.6. [Dy(K-HOEt)(L)₄]₂

M.p. 262–263 °C; elemental Anal. Calcd (%) for C₁₈₀H₁₃₂Dy₂K₂O₂₆: C, 69.42; H, 4.27; found: C, 69.60; H, 3.78; ATR-IR: $\nu = 3650$ w, 3563 w, 3055 w, 3019 w, 2972 w, 1645 m, 1609 w, 1584 m, 1545 s, 1490 m, 1447 m, 1371 s, 1310 m, 1279 m, 1193 w, 1177 w, 1151 m, 1072 w, 1028 w, 1010 w, 975 w, 927 w, 898 m, 824 w, 780 w, 749 m, 694 m, 668 cm⁻¹ w.

4.3.7. [Dy(Rb-HOEt)(L)₄]₂

M.p. 267–268 °C; elemental Anal. Calcd (%) for C₁₈₀H₁₃₂Dy₂Rb₂O₂₆·0.5(H₂O): C, 67.23; H, 4.17; found: C, 66.81; H, 3.59; the elemental analysis deviates somewhat from the theoretical values, possibly due to the presence of multiple solvates; ATR-IR: $\nu = 3653$ w, 3571 w, 3057 w, 1645 m, 1611 w, 1584 s, 1545 s, 1491 m, 1447 m, 1373 s, 1311 m, 1277 m, 1178 w, 1151 m, 1073 w, 1027 w, 1013 w, 999 w, 976 w, 925 w, 898 m, 823 w, 812 w, 780 w, 748 m, 694 m, 668 cm⁻¹ w.

4.3.8. [Ho(K-HOEt)(L)₄]₂

M.p. 260–261 °C; elemental Anal. Calcd (%) for C₁₈₀H₁₃₂Ho₂K₂O₂₆: C, 69.31; H, 4.27; found: C, 69.11; H, 3.87; ATR-IR: $\nu = 3567$ w, 3059 w, 3019 w, 2968 w, 1668 m, 1644 m, 1611 w, 1584 s, 1546 s, 1490 m, 1447 m, 1389 s, 1371 s, 1310 m, 1279 m, 1195 w, 1180 w, 1179 w, 1151 m, 1074 w, 1024 w, 1012 w, 999 w, 927 w, 898 m, 840 w, 823 w, 778 w, 749 m, 749 w, 694 m, 668 cm⁻¹ w.

4.3.9. [Ho(Rb-HOEt)(L)₄]₂

M.p. 268–270 °C; elemental Anal. Calcd (%) for C₁₈₀H₁₃₂Ho₂Rb₂O₂₆: C, 67.31; H, 4.14; found: C, 66.84; H, 3.68; ATR-IR: ν = 3660 w, 3570 w, 3056 w, 1645 m, 1612 w, 1584 s, 1548 s, 1492 m, 1447 m, 1373 s, 1311 m, 1278 m, 1179 w, 1151 m, 1073 w, 1027 w, 1013 w, 999 w, 976 w, 924 w, 897 m, 824 w, 780 w, 749 m, 695 m, 669 cm⁻¹ w.

4.4. X-ray crystallography

Crystallographic data for the structures were collected at 100(2) K on an Oxford Diffraction Gemini or Xcalibur diffractometer fitted with Mo K α or Cu K α radiation. Following absorption corrections and solution by direct methods, the structures were refined against F^2 with full-matrix least-squares using SHELXL-97 or SHELX-2014 [25]. Unless stated below, anisotropic displacement parameters were employed for the non-hydrogen atoms. Except for some ethanol hydrogens, all hydrogen atoms were added at calculated positions and refined by use of a riding model with isotropic displacement parameters based on those of the parent atom. CCDC-1443572 [Gd(K-HOEt)(L)₄]₂, CCDC-1443573 [Gd(Rb-HOEt)(L)₄]₂, CCDC-1443574 [Tb(Na-HOEt)(L)₄]₂, CCDC-1443575 [Tb(K-HOEt)(L)₄]₂, CCDC-1443576 [Tb(Rb-HOEt)(L)₄]₂, CCDC-1443577 [Dy(K-HOEt)(L)₄]₂, CCDC-1443578 [Dy(K-HOEt)(L)₄]₂·2EtOH, CCDC-1443579 [Dy(Rb-HOEt)(L)₄]₂, CCDC-1443580 [Ho(K-HOEt)(L)₄]₂, and CCDC-1443581 [Ho(Rb-HOEt)(L)₄]₂ contain supplementary crystallographic data and can be obtained free of charge via <http://www.ccdc.cam.ac.uk/conts/retrieving.html>, or from the Cambridge Crystallographic Data Center, 12 Union Road, Cambridge CB2 1EZ, UK; Fax: (+44) 1223-336-033; or E-mail: deposit@ccdc.cam.ac.uk.

4.5. X-ray data refinement

4.5.1. [Gd(K-HOEt)(L)₄]₂·2EtOH

Empirical formula C₁₈₄H₁₄₄Gd₂K₂O₂₈; MW = 3195.68. Triclinic, space group $P\bar{1}$, a = 13.9309(3), b = 14.8457(3), c = 19.6249(5) Å, α = 80.167(2)°, β = 72.496(2)°, γ = 90.110(2)°, Volume = 3807.77(16) Å³, Z = 1; ρ_c = 1.394 Mg m⁻³, μ = 0.993 mm⁻¹, crystal size 0.53 × 0.29 × 0.21 mm³; $\theta_{\min, \max}$ = 2.04, 34.00°. Reflections collected = 120,523, unique reflections = 31,054 [$R(\text{int})$ = 0.0428]. Max. and min. transmission = 0.842 and 0.728. Number of parameters = 1087, S = 1.061; Final R indices [$I > 2\sigma(I)$] $R1$ = 0.0345, $wR2$ = 0.0791; R indices (all data) $R1$ = 0.0419, $wR2$ = 0.0824; Largest diff. peak and hole 2.032 and -1.195 eÅ⁻³. One phenyl ring and both the coordinated and uncoordinated ethanol solvent molecules were modeled as being disordered over two sets of sites with occupancies constrained to 0.5 after trial refinement. The coordinated ethanol OH hydrogens were not located.

4.5.2. [Gd(Rb-HOEt)(L)₄]₂·2EtOH

Empirical formula C₁₈₄H₁₄₄Gd₂Rb₂O₂₈; MW = 3288.42. Triclinic, space group $P\bar{1}$, a = 14.0074(3), b = 14.8085(4), c = 19.7192(4) Å, α = 80.083(2)°, β = 72.374(2)°, γ = 90.044(2)°, Volume = 3833.95(16) Å³, Z = 1; ρ_c = 1.424 Mg m⁻³, μ = 1.563 mm⁻¹, crystal size 0.31 × 0.22 × 0.16 mm³; $\theta_{\min, \max}$ = 2.80, 31.97°. Reflections collected = 47,040, unique reflections = 24,546 [$R(\text{int})$ = 0.0284]. Max. and min. transmission = 0.810 and 0.696. Number of parameters = 1093, S = 1.033; Final R indices [$I > 2\sigma(I)$] $R1$ = 0.0366, $wR2$ = 0.0829; R indices (all data) $R1$ = 0.0453, $wR2$ = 0.0873; Largest diff. peak and hole 1.828 and -1.375 eÅ⁻³. One phenyl ring and both the coordinated and uncoordinated ethanol solvent molecules were modeled as being disordered over two sets of sites with occupancies constrained to 0.5 after trial refinement. The ethanol OH hydrogen positions were refined with geometries restrained to ideal values.

4.5.3. [Tb(Na-HOEt)(L)₄]₂

Empirical formula C₁₈₀H₁₃₂Tb₂Na₂O₂₆; MW = 3074.68. Triclinic, space group $P\bar{1}$, a = 13.8911(8), b = 14.6303(6), c = 18.0785(8) Å, α = 104.868(4)°, β = 90.597(4)°, γ = 89.885(4)°, Volume = 3550.9(3) Å³, Z = 1; ρ_c = 1.438 Mg m⁻³, λ = 1.54178 Å, μ = 5.516 mm⁻¹, crystal size 0.25 × 0.09 × 0.07 mm³; $\theta_{\min, \max}$ = 3.13, 67.34°. Reflections collected = 34,110, unique reflections = 12,611 [$R(\text{int})$ = 0.0645]. Max. and

min. transmission = 0.728 and 0.389. Number of parameters = 946, $S = 1.030$; Final R indices [$I > 2\sigma(I)$] $R1 = 0.0519$, $wR2 = 0.1267$; R indices (all data) $R1 = 0.0629$, $wR2 = 0.1366$; Largest diff. peak and hole 2.023 and $-0.963 \text{ e}\text{\AA}^{-3}$.

4.5.4. [Tb(K-HOEt)(L)₄]₂

Empirical formula $\text{C}_{180}\text{H}_{132}\text{K}_2\text{O}_{26}\text{Tb}_2$; $MW = 3106.89$. Triclinic, space group $P\bar{1}$, $a = 13.9716(3)$, $b = 14.5463(5)$, $c = 18.1001(4) \text{ \AA}$, $\alpha = 103.116(2)^\circ$, $\beta = 89.996(2)^\circ$, $\gamma = 89.797(2)^\circ$, Volume = $3582.59(17) \text{ \AA}^3$, $Z = 1$; $\rho_c = 1.440 \text{ Mg m}^{-3}$, $\mu = 1.114 \text{ mm}^{-1}$, crystal size $0.420 \times 0.175 \times 0.088 \text{ mm}^3$; $\theta_{\text{min,max}} = 2.04, 28.00^\circ$. Reflections collected = 30,660, unique reflections = 17,248 [$R(\text{int}) = 0.0308$]. Max. and min. transmission = 0.911 and 0.700. Number of parameters = 946, $S = 1.052$; Final R indices [$I > 2\sigma(I)$] $R1 = 0.0494$, $wR2 = 0.1056$; R indices (all data) $R1 = 0.0628$, $wR2 = 0.1115$; Largest diff. peak and hole 2.749 and $-1.660 \text{ e}\text{\AA}^{-3}$. The ethanol OH hydrogen was not located.

4.5.5. [Tb(Rb-HOEt)(L)₄]₂·2EtOH

Empirical formula $\text{C}_{184}\text{H}_{144}\text{Tb}_2\text{Rb}_2\text{O}_{28}$; $MW = 3243.73$. Triclinic, space group $P\bar{1}$, $a = 13.9918(2)$, $b = 14.7907(6)$, $c = 19.7441(3) \text{ \AA}$, $\alpha = 80.170(1)^\circ$, $\beta = 72.319(1)^\circ$, $\gamma = 90.086(1)^\circ$, Volume = $3829.65(11) \text{ \AA}^3$, $Z = 1$; $\rho_c = 1.406 \text{ Mg m}^{-3}$, $\mu = 1.621 \text{ mm}^{-1}$, crystal size $0.47 \times 0.44 \times 0.28 \text{ mm}^3$; $\theta_{\text{min,max}} = 2.14, 41.15^\circ$. Reflections collected = 160,326, unique reflections = 49,625 [$R(\text{int}) = 0.0445$]. Max. and min. transmission = 0.703 and 0.526. Number of parameters = 1081, $S = 1.004$; Final R indices [$I > 2\sigma(I)$] $R1 = 0.0355$, $wR2 = 0.0693$; R indices (all data) $R1 = 0.0502$, $wR2 = 0.0742$; Largest diff. peak and hole 1.880 and $-1.056 \text{ e}\text{\AA}^{-3}$. One phenyl ring and both the coordinated and uncoordinated ethanol solvent molecules were modeled as being disordered over two sets of sites with occupancies constrained to 0.5 after trial refinement. Hydrogens on ethanol oxygens were not located.

4.5.6. [Dy(K-HOEt)(L)₄]₂

Empirical formula $\text{C}_{180}\text{H}_{132}\text{Dy}_2\text{K}_2\text{O}_{26}$; $MW = 3114.06$. Triclinic, space group $P\bar{1}$, $a = 13.9658(4)$, $b = 14.5111(4)$, $c = 18.0746(5) \text{ \AA}$, $\alpha = 103.049(2)^\circ$, $\beta = 90.026(2)^\circ$, $\gamma = 89.566(2)^\circ$, Volume = $3568.29(17) \text{ \AA}^3$, $Z = 1$; $\rho_c = 1.449 \text{ Mg m}^{-3}$, $\mu = 1.174 \text{ mm}^{-1}$, crystal size $0.24 \times 0.21 \times 0.10 \text{ mm}^3$; $\theta_{\text{min,max}} = 2.83, 30.00^\circ$. Reflections collected = 85,194, unique reflections = 20,748 [$R(\text{int}) = 0.0582$]. Max. and min. transmission = 0.895 and 0.823. Number of parameters = 947, $S = 1.157$; Final R indices [$I > 2\sigma(I)$] $R1 = 0.0701$, $wR2 = 0.1635$; R indices (all data) $R1 = 0.0807$, $wR2 = 0.1681$; Largest diff. peak and hole 4.190 and $-1.589 \text{ e}\text{\AA}^{-3}$. The ethanol OH hydrogen was not located.

4.5.7. [Dy(K-HOEt)(L)₄]₂·2EtOH

Empirical formula $\text{C}_{184}\text{H}_{144}\text{Dy}_2\text{K}_2\text{O}_{28}$; $MW = 3206.19$. Triclinic, space group $P\bar{1}$, $a = 13.9132(5)$, $b = 14.8410(8)$, $c = 19.6256(8) \text{ \AA}$, $\alpha = 80.221(4)^\circ$, $\beta = 72.392(4)^\circ$, $\gamma = 89.987(4)^\circ$, Volume = $3800.8(3) \text{ \AA}^3$, $Z = 1$; $\rho_c = 1.401 \text{ Mg m}^{-3}$, $\mu = 1.105 \text{ mm}^{-1}$, crystal size $0.21 \times 0.11 \times 0.04 \text{ mm}^3$; $\theta_{\text{min,max}} = 2.79, 27.00^\circ$. Reflections collected = 27,980, unique reflections = 16,193 [$R(\text{int}) = 0.0374$]. Max. and min. transmission = 0.959 and 0.764. Number of parameters = 1081, $S = 0.993$; Final R indices [$I > 2\sigma(I)$] $R1 = 0.0417$, $wR2 = 0.0861$; R indices (all data) $R1 = 0.0529$, $wR2 = 0.0908$; Largest diff. peak and hole 0.992 and $-1.054 \text{ e}\text{\AA}^{-3}$. One phenyl ring and both the coordinated and uncoordinated ethanol solvent molecules were modeled as being disordered over two sets of sites with occupancies constrained to 0.5 after trial refinement. The ethanol OH hydrogens were not located.

4.5.8. [Dy(Rb-HOEt)(L)₄]₂·2EtOH

Empirical formula $\text{C}_{184}\text{H}_{144}\text{Dy}_2\text{Rb}_2\text{O}_{28}$; $MW = 3298.93$. Triclinic, space group $P\bar{1}$, $a = 13.9581(3)$, $b = 14.7899(3)$, $c = 19.7191(3) \text{ \AA}$, $\alpha = 80.097(2)^\circ$, $\beta = 72.276(2)^\circ$, $\gamma = 90.065(2)^\circ$, Volume = $3813.58(13) \text{ \AA}^3$, $Z = 1$; $\rho_c = 1.436 \text{ Mg m}^{-3}$, $\mu = 1.681 \text{ mm}^{-1}$, crystal size $0.28 \times 0.19 \times 0.11 \text{ mm}^3$; $\theta_{\text{min,max}} = 2.80, 35.94^\circ$. Reflections collected = 113,525, unique reflections = 34,619 [$R(\text{int}) = 0.0619$]. Max. and min. transmission = 0.868 and 0.722. Number of parameters = 1081, $S = 1.092$; Final R indices [$I > 2\sigma(I)$] $R1 = 0.0537$, $wR2 = 0.1071$; R indices (all data) $R1 = 0.0703$, $wR2 = 0.1136$; Largest diff. peak and hole 3.134 and

$-1.253 \text{ e}\text{\AA}^{-3}$. One phenyl ring and both the coordinated and uncoordinated ethanol solvent molecules were modeled as being disordered over two sets of sites. The ethanol OH hydrogens were not located.

4.5.9. [Ho(K-HOEt)(L)₄]₂

Empirical formula $\text{C}_{180}\text{H}_{132}\text{Ho}_2\text{K}_2\text{O}_{26}$; $MW = 3118.92$. Triclinic, space group $P\bar{1}$, $a = 14.0116(4)$, $b = 14.5056(3)$, $c = 18.0275(4)$ Å, $\alpha = 102.746(2)^\circ$, $\beta = 90.006(2)^\circ$, $\gamma = 89.190(2)^\circ$, Volume = $3573.36(15)$ Å³, $Z = 1$; $\rho_c = 1.449 \text{ Mg m}^{-3}$, $\mu = 1.234 \text{ mm}^{-1}$, crystal size $0.59 \times 0.43 \times 0.19 \text{ mm}^3$; $\theta_{\text{min,max}} = 2.84, 30.00^\circ$. Reflections collected = 96,102, unique reflections = 20,828 [$R(\text{int}) = 0.0415$]. Max. and min. transmission = 0.799 and 0.588. Number of parameters = 946, $S = 1.063$; Final R indices [$I > 2\sigma(I)$] $R1 = 0.0354$, $wR2 = 0.0878$; R indices (all data) $R1 = 0.0392$, $wR2 = 0.0904$; Largest diff. peak and hole 2.303 and $-1.233 \text{ e}\text{\AA}^{-3}$. The ethanol OH hydrogen was not located with sufficient confidence to be included in the model.

4.5.10. [Ho(Rb-HOEt)(L)₄]₂·2EtOH

Empirical formula $\text{C}_{184}\text{H}_{144}\text{Ho}_2\text{Rb}_2\text{O}_{28}$; $MW = 3303.79$. Triclinic, space group $P\bar{1}$, $a = 13.9449(8)$, $b = 14.7815(6)$, $c = 19.7069(11)$ Å, $\alpha = 80.013(4)^\circ$, $\beta = 72.296(5)^\circ$, $\gamma = 90.008(4)^\circ$, Volume = $3805.0(3)$ Å³, $Z = 1$; $\rho_c = 1.442 \text{ Mg m}^{-3}$, $\mu = 1.743 \text{ mm}^{-1}$, crystal size $0.21 \times 0.09 \times 0.045 \text{ mm}^3$; $\theta_{\text{min,max}} = 2.14, 28.34^\circ$. Reflections collected = 28,503, unique reflections = 16,616 [$R(\text{int}) = 0.0493$]. Max. and min. transmission = 0.963 and 0.855. Number of parameters = 1021, $S = 1.023$; Final R indices [$I > 2\sigma(I)$] $R1 = 0.0528$, $wR2 = 0.0811$; R indices (all data) $R1 = 0.0767$, $wR2 = 0.0891$; Largest diff. peak and hole 1.027 and $-0.924 \text{ e}\text{\AA}^{-3}$. One phenyl ring, and both the coordinated and uncoordinated ethanol solvent molecules were modeled as being disordered over two sets of sites with occupancies constrained to 0.5 after trial refinement. Disordered atoms were refined with isotropic displacement parameters. Hydrogens on the ethanol oxygens were not located.

Supplementary material

The Supporting Information contains molecular displacement plots of all assemblies not presented herein and raw Ln–O distances for all crystal structures.

Acknowledgements

M.M. wishes to thank the ARC for funding (FT130100033). B.L.R. wishes to thank Curtin University for the Australian Postgraduate Award. The authors acknowledge access to the facilities at the Centre for Microscopy, Characterisation and Analysis, University of Western Australia.

Disclosure statement

No potential conflict of interest was reported by the authors.

Funding

This work was supported by ARC [grant number FT130100033].

References

- [1] J.-C.G. Bünzli. *Coord. Chem. Rev.*, **293-294**, 19 (2015).
- [2] M.A. Katkova, M.N. Bochkarev. *Dalton Trans.*, **39**, 6599 (2010).
- [3] J.-C.G. Bünzli. *Acc. Chem. Res.*, **39**, 53 (2006).
- [4] J.-C.G. Bünzli, S.V. Eliseeva. *J. Rare Earths*, **28**, 824 (2010).
- [5] S.V. Eliseeva, J.-C.G. Bünzli. *New J. Chem.*, **35**, 1165 (2011).
- [6] R. Sessoli, A.K. Powell. *Coord. Chem. Rev.*, **253**, 2328 (2009).
- [7] S. Faulkner, S.J.A. Pope, B.P. Burton-Pye. *Appl. Spectrosc. Rev.*, **40**, 1 (2005).
- [8] J.-C.G. Bünzli. *J. Lumin.*, **170**, 866 (2016).

- [9] P.C. Andrews, W.J. Gee, P.C. Junk, M. Massi. *New J. Chem.*, **37**, 35 (2013).
- [10] K. Binnemans. In *Handbook on the Physics and Chemistry of Rare Earths*, K.A. Gschneidner, J.-C.G. Bunzli, V.J. Pecharsky (Eds), pp. 107–272, Elsevier B.V., Amsterdam (2005).
- [11] D.T. Thielemann, A.T. Wagner, Y. Lan, P. Oña-Burgos, I. Fernández, E.S. Rösch, D.K. Kölmel, A.K. Powell, S. Bräse, P.W. Roesky. *Chem. Eur. J.*, **21**, 2813 (2015).
- [12] D.T. Thielemann, A.T. Wagner, E. Rösch, D.K. Kölmel, J.G. Heck, B. Rudat, M. Neumaier, C. Feldmann, U. Schepers, S. Bräse, P.W. Roesky. *J. Am. Chem. Soc.*, **135**, 7454 (2013).
- [13] M. Ismail, S.J. Lyle, J.E. Newbery. *J. Inorg. Nucl. Chem.*, **31**, 2091 (1969).
- [14] G.A. Crosby, R.E. Whan. *J. Chem. Phys.*, **32**, 614 (1960).
- [15] G.A. Crosby, R.E. Whan, R.M. Alire. *J. Chem. Phys.*, **34**, 743 (1961).
- [16] B.L. Reid, S. Stagni, J.M. Malicka, M. Cocchi, G.S. Hanan, M.I. Ogden, M. Massi. *Chem. Commun.*, **50**, 11580 (2014).
- [17] B.L. Reid, S. Stagni, J.M. Malicka, M. Cocchi, A.N. Sobolev, B.W. Skelton, E.G. Moore, G.S. Hanan, M.I. Ogden, M. Massi. *Chem. Eur. J.*, **21**, 18354 (2015).
- [18] S. Demir, J.M. Zadrozny, M. Nippe, J.R. Long. *J. Am. Chem. Soc.*, **134**, 18546 (2012).
- [19] J.D. Rinehart, M. Fang, W.J. Evans, J.R. Long. *Nat. Chem.*, **3**, 538 (2011).
- [20] M. Llunell, D. Casanova, J. Cirera, P. Alemany, S. Alvarez. Shape version 2.1. Available online at: <http://www.ee.ub.es/index.php/news-ee/575-shape-available> (2013).
- [21] D. Casanova, M. Llunell, P. Alemany, S. Alvarez. *Chem. Eur. J.*, **11**, 1479 (2005).
- [22] J. Tang, I. Hewitt, N.T. Madhu, G. Chastanet, W. Wernsdorfer, C.E. Anson, C. Benelli, R. Sessoli, A.K. Powell. *Angew. Chem. Int. Ed.*, **45**, 1729 (2006).
- [23] M.L. Kahn, J.-P. Sutter, S. Golhen, P. Guionneau, L. Ouahab, O. Kahn, D. Chasseau. *J. Am. Chem. Soc.*, **122**, 3413 (2000).
- [24] V.S. Sastri, J.-C.G. Bünzli, V.R. Rao, G.V.S. Rayudu, J.R. Perumareddi. *Modern Aspects of Rare Earths and their Complexes*, pp. 259–374, Elsevier, Amsterdam (2003).
- [25] G.M. Sheldrick. *Acta Crystallogr., Sect. C*, **71**, 3 (2015).